Check for updates

Received: 2 August 2022 | Revised: 13 December 2022 | Accepted: 14 December 2022 | Published on: 9 January 2023

DOI: 10.1002/mrm.29569

RESEARCH ARTICLE

Magnetic Resonance in Medicine

The effects of RF coils and SAR supervision strategies for clinically applicable nonselective parallel-transmit pulses at 7 T

Jürgen Herrler[1,2] | **Sydney N. Williams**[3] | **Patrick Liebig**[2] | **Belinda Ding**[4] | **Paul McElhinney**[3] | **Sarah Allwood-Spiers**[5] | **Christian R. Meixner**[2,6] | **Shajan Gunamony**[3,7] | **Andreas Maier**[8] | **Arnd Dörfler**[1] | **Rene Gumbrecht**[2] | **David A. Porter**[3] | **Armin M. Nagel**[6,9]

[1]Department of Neuroradiology, University Hospital Erlangen, Friedrich-Alexander-Universität Erlangen-Nürnberg, Erlangen, Germany

[2]Siemens Healthcare, Erlangen, Germany

[3]Imaging Center of Excellence, University of Glasgow, Glasgow, UK

[4]Siemens Healthcare, Frimley, UK

[5]National Health Service Greater Glasgow & Clyde, Glasgow, UK

[6]Institute of Radiology, University Hospital Erlangen, Friedrich-Alexander-Universität Erlangen-Nürnberg, Erlangen, Germany

[7]MR CoilTech, Glasgow, UK

[8]Department of Computer Science, Friedrich-Alexander-Universität Erlangen-Nürnberg, Erlangen, Germany

[9]Division of Medical Physics in Radiology, German Cancer Research Center, Heidelberg, Germany

Correspondence
Jürgen Herrler, Department of Neuroradiology, University Hospital Erlangen, Friedrich-Alexander-Universität Erlangen-Nürnberg, Maximiliansplatz 2, 91054, Erlangen, Germany.
Email: juergen.herrler@siemens-healthineers.com

Funding information
NHS Greater Glasgow & Clyde, Glasgow, UK

Purpose: To investigate the effects of using different parallel-transmit (pTx) head coils and specific absorption rate (SAR) supervision strategies on pTx pulse design for ultrahigh-field MRI using a 3D-MPRAGE sequence.

Methods: The PTx universal pulses (UPs) and fast online-customized (FOCUS) pulses were designed with pre-acquired data sets (B_0, B_1^+ maps, specific absorption rate [SAR] supervision data) from two different 8 transmit/32 receive head coils on two 7T whole-body MR systems. For one coil, the SAR supervision model consisted of per-channel RF power limits. In the other coil, SAR estimations were done with both per-channel RF power limits as well as virtual observation points (VOPs) derived from electromagnetic field (EMF) simulations using three virtual human body models at three different positions. All pulses were made for nonselective excitation and inversion and evaluated on 132 B_0, B_1^+, and SAR supervision datasets obtained with one coil and 12 from the other. At both sites, 3 subjects were examined using MPRAGE sequences that used UP/FOCUS pulses generated for both coils.

Results: For some subjects, the UPs underperformed when simulated on a different coil from which they were derived, whereas FOCUS pulses still showed acceptable performance in that case. FOCUS inversion pulses outperformed adiabatic pulses when scaled to the same local SAR level. For the self-built coil, the use of VOPs showed reliable overestimation compared with the ground-truth EMF simulations, predicting about 52% lower local SAR for inversion pulses compared with per-channel power limits.

Conclusion: FOCUS inversion pulses offer a low-SAR alternative to adiabatic pulses and benefit from using EMF-based VOPs for SAR estimation.

KEYWORDS
fast online customized (FOCUS) pulses, parallel transmission (pTx), radiofrequency (RF) coils, UHF MRI, universal pulses (UPs), virtual observation points (VOPs)

Jürgen Herrler and Sydney N. Williams contributed equally to this work.

This is an open access article under the terms of the Creative Commons Attribution License, which permits use, distribution and reproduction in any medium, provided the original work is properly cited.
© 2023 The Authors. *Magnetic Resonance in Medicine* published by Wiley Periodicals LLC on behalf of International Society for Magnetic Resonance in Medicine.

1 | INTRODUCTION

MRI at ultrahigh fields (UHF, static magnetic field $B_0 \geq 7$ T) has shown great potential for improving image quality through increased SNR, and in many cases, improved image contrast.[1] However, the increased spatial variation in the transmit (Tx) RF field (B_1^+) results in corresponding inhomogeneous flip angle (FA) distributions when using conventional circularly polarized (CP) pulses. Parallel-transmit (pTx) pulses use multiple Tx channels, which can be driven with their own unique RF pulse form. The B_1^+ field emerges as interference of the fields generated by the independent channels and is manipulated by the choice of their corresponding RF pulse forms.

Dynamic pTx pulses use channel-specific pulse shapes, generating temporally varying B_1^+ fields. Throughout RF excitation, the phase of the preceding nuclear spins is affected by B_0 inhomogeneities but can additionally be manipulated by using complementary gradient fields.[2,3] In total, dynamic pTx pulses offer more degrees of freedom for pulse design and thus a higher potential to produce more homogeneous FA distributions. These pulses are an essential requirement for generating uniform RF signal over the entirety of the head at 7 T[1] but have not been used in regular clinical practice yet.

Routine clinical use of dynamic pTx is often burdened by its complex optimization workflow. One major step toward clinical application is the concept of universal pulses (UPs),[4] which have been presented for various 3D pulse sequences in the head,[5,6] and the heart.[7] These pulses are designed using pre-acquired B_1^+ and B_0 maps from a group of subjects and significantly improve the FA homogeneity for unseen test cases compared with CP pulses. Because individually optimized pulses can further improve pulse performance, the concepts of standardized UPs (SUPs)[8] and fast online-customized (FOCUS) pulses have been proposed.[9] These two approaches consist of a universal optimization of pulses and parameters before the scan and a subsequent individual optimization during the actual scan with acquired subject-specific field maps. SUPs use three-slice B_1^+ maps acquired in < 10 s to derive a linear transformation of the predesigned universal RF pulse shapes. FOCUS pulses currently use B_1^+ and B_0 maps across the whole volume in 47 s to perform a more comprehensive individual optimization of the pulses. UPs have also been proposed for large FAs and have shown to work on multiple commercially available coils[10] yet are designed to be used on distinct coil designs. On the contrary, FOCUS pulses have so far only been shown for small FAs, designed using the small-tip-angle (STA) approximation,[2] and only on one pTx coil. To broaden the application of FOCUS pulses, we extend this concept beyond the saturation pulse (STA) approximation by generating 180° inversion pulses and evaluating their use on two pTx head coils.

Another challenge of UHF MRI is the increased specific absorption rate (SAR) exposure due to larger RF power requirements and its stronger local variation with reduced RF wavelength.[11] Furthermore, because parallel transmission allows for varying amplitude and phase relationships between transmit elements, it is not sufficient to consider power absorbed by the entire body region and instead must be monitored locally in 10-g volumes.[12] This detailed monitoring of local SAR exposure is regulated for UHF with limits specified by the International Electrotechnical Commission (IEC) guideline 60 601–2-33.[13]

Evaluation of local SAR with pTx requires electromagnetic field (EMF) simulations of the pTx RF coil using digital human body models. Given a 3D spatial distribution of conductivity, density, and electric fields, a body model simulation can be formulated into a set of so-called "Q-matrices," enabling a simple quadratic relationship between an applied multichannel voltage and local SAR.[14] Nevertheless, estimation of local SAR remains computationally demanding, with EMF simulations often exceeding millions of voxels. A common solution for tractable local SAR estimation is by using virtual observation points (VOPs), which compress a large set of simulation Q-matrices into a smaller set of clustered local SAR points.[15] VOPs are bounded by a percent overestimation with respect to a calculated "worst case" excitation vector, determined as the eigenvector associated with the largest eigenvalue of all VOPs. When generated from a diverse and realistic population of body model EMF simulations, VOPs are bounded above the true Q-matrices' local SAR for a particular pTx coil.

Another method for monitoring local SAR with pTx is to directly limit the peak RF power per transmit channel. In this scenario, the eigenvector from the largest eigenvalue of the full simulation set of Q-matrices (the ground truth "worst case") is used to determine the power limit. The power required to generate a specific local SAR threshold (such as IEC operating normal mode limits of 10 W/kg[13]) is set as the upper limit for all channels. This again ensures no underestimation of SAR, but these per-channel power limits can be conservative for some applications. Nevertheless, such limits are often desirable for applications outside the brain such as in the body, where peak SAR values vary greatly with subject size and anatomy.[7]

This work explores both the pTx topics of B_1^+ field homogenization and local SAR monitoring with comparisons in two coils each containing 8-Tx and 32–receive (Rx) elements: one commercially available and one self-built. For both coils, UPs and FOCUS pulses were generated for excitation and inversion. These pulses were used

15222594, 2023, 5, Downloaded from https://onlinelibrary.wiley.com/doi/10.1002/mrm.29569 by Universidad Rey Juan Carlos C/Tulipan S/N Edificio, Wiley Online Library on [24/01/2025]. See the Terms and Conditions (https://onlinelibrary.wiley.com/terms-and-conditions) on Wiley Online Library for rules of use; OA articles are governed by the applicable Creative Commons License

experimentally in healthy volunteers in a 3D T_1-weighted MPRAGE sequence.[16] The performance of these pulses was compared across coils in terms of normalized RMS error (NRMSE) and their local SAR contributions based on EMF-based VOP estimates and per-channel power estimates.

2 | METHODS

2.1 | Measurement system and data acquisition

All measurements were conducted as a multisite study at the University Hospital Erlangen and the Imaging Center of Excellence in Glasgow on two 7T whole-body MR systems (MAGNETOM Terra; Siemens Healthcare, Erlangen, Germany) with one commercially available 8-Tx/32-Rx head coil (Nova Medical, Wilmington, DE, USA) and one self-built 8-Tx/32-Rx head coil[17] in Erlangen and in Glasgow, respectively. Both coils were previously observed to have similar B_1^+ performance, yet unlike the commercially available coil, the self-built coil also has eye cut-outs for subject comfort.[17] SAR supervision was managed with fixed per-channel power limits for the commercial coil and the self-built coil with an EMF-based VOP model described subsequently. B_1^+/B_0 maps were acquired in the sequence preparation phase of any sequence using FOCUS pTx pulses. B_0 mapping was performed with a sagittal GRE sequence (TE_1 = 1.02 ms; TE_2 = 3.06 ms; resolution = 4.41 mm^3 isotropic; 52 slices; 0.88-mm slice gapping; FOV = 282 × 282 × 274 mm^3; acquisition time [TA] = 9.6 s). B_1^+ mapping was performed using a transverse interferometric magnetization-prepared saturation recovery turbo FLASH sequence (TE = 1.63 ms; TR = 3.75 s; resolution = 4 × 4 × 5 mm^3; 25 slices; 5-mm slice gapping; FOV = 256 × 256 × 245; TA = 35 s).[18]

All pTx pulses were used in a sagittal 3D-MPRAGE prototype sequence. The following timing parameters were applied based on the established clinical T_1-weighted protocols from both sites: FA = 5°, TR = 3 s, TI = 1.1 s, TA = 4 min 56 s, TE = 3.19 ms, FOV = 250 × 226 × 160 mm^3, 1-mm^3 isotropic resolution, readout bandwidth = 250 Hz/Px, GRAPPA acceleration factor 3, and echo spacing (ES) = 6.9 ms using CP rectangular-shaped pulses and ES = 7.8 ms using pTx pulses. All previously acquired B_1^+ and B_0 maps used for pulse design were interpolated into a 4 × 4 × 6 mm^3 matrix in sagittal orientation covering the FOV of the sequence.

Furthermore, a second 3D-MPRAGE protocol was created with 0.5-mm^3 isotropic resolution by doubling the previous scan matrix size. Due to SAR limitations, this additional scan was only performed in the self-built coil. The only other sequence parameters that were adjusted to accommodate the higher resolution were TI = 1.37 s, TA = 9 min 15 s, bandwidth = 515 Hz/Px, and ES = 6.7 ms.

Before the study, pTx pulses were generated using eight training data sets each from both the commercially available and the self-built coils, which consisted of subject-specific B_1^+ and B_0 maps and coil-specific local SAR estimation methods. For each coil, excitation and inversion pTx pulses were generated to use as UPs or as the initialization for FOCUS pulses and denoted accordingly as $UP_{com/sb,\ ChPowLim/EMF}$/$FOCUS_{com/sb,\ ChPowLim/EMF}$. Figure 1 shows an overview of the generated pulses for the two RF coils and corresponding SAR supervision strategies.

These pulses were evaluated on 132 data sets previously acquired with the commercially available coil and 12 data sets previously acquired with the self-built coil by performing Bloch simulations and SAR calculations derived from the respective VOP models. Three subjects, included in these evaluation data sets, were examined experimentally with prospective data collection using the commercially available coil and the 3D-MPRAGE sequence. Excitation and inversion pulses were designed for both pTx coils: $UP/FOCUS_{com}$ or $UP/FOCUS_{sb}$. Similarly, 3 additional subjects not included in the evaluation data sets were examined with the same MPRAGE sequences using the self-built coil. One of those subjects was scanned at both sites.

The study was approved by the local ethical review boards, and all subjects provided informed consent before the scan at both sites.

2.2 | SAR management

Local SAR monitoring is specific to each unique pTx coil, and in this study, the primary local SAR estimation methods were different for the two. For the commercial coil, fixed, per-channel power limits were used as provided by the coil manufacturer. This equates to eight real-valued local SAR checkpoints for every complex pTx configuration, one for each transmit elements. For the self-built coil, local SAR was monitored with VOPs derived from the coil's EMF simulation (CST Studio Suite; Dassault Systems, France). The VOP file was generated by concatenating nine data sets consisting of three body models, with each model placed in three positions along the z-direction in 10-mm increments. The VOPs were compressed with a 25% overestimation factor with respect to "worst case" configuration using the method in Eichfelder and Gebhardt,[15] yielding a total of 15 complex VOP checkpoints. Furthermore, cable loss and an additional term to account for scanner manufacturer–recommended RF supervision

15222594, 2023, 5, Downloaded from https://onlinelibrary.wiley.com/doi/10.1002/mrm.29569 by Universidad Rey Juan Carlos C/Tulipan S/N Edificio, Wiley Online Library on [24/01/2025]. See the Terms and Conditions (https://onlinelibrary.wiley.com/terms-and-conditions) on Wiley Online Library for rules of use; OA articles are governed by the applicable Creative Commons License

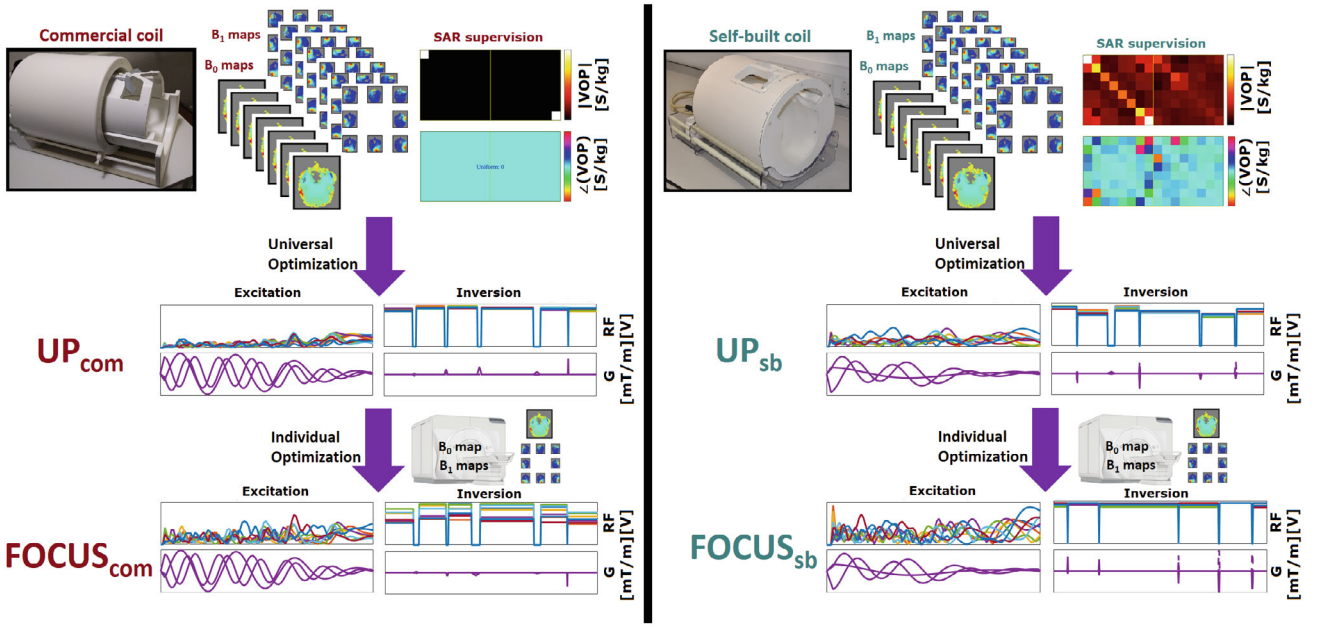

FIGURE 1 One commercial and one self-built coil were used for the measurements. Universal pulses (UPs) and corresponding parameters (energy regularization weight for excitation pulses, specific energy dose [SED] limit for inversion pulses) were generated for both coils using eight different B_1^+ and B_0 maps as well as coil-specific specific absorption rate (SAR) supervision matrices (first and last virtual observation points [VOP] matrix). Fast online-customized (FOCUS) pulses were then generated based on the actual subject's B_1^+ and B_0 maps acquired during the scan

system errors was included. In total, these terms yielded a combined safety factor of 1.7.[17] A final scaling factor of 1.2 was included, giving an overall safety factor of 2.04.[19]

To facilitate the comparison across the two coils with distinct SAR management methods, a set of per-channel power limits was also derived for the self-built coil as an alternative form of SAR supervision. Using the full simulation Q-matrices, the power limit was set to 0.78 W per channel, which would limit the peak local SAR to 10 W/kg for the "worst case" transmit configuration. Unlike the EMF-based supervision, the fixed per-channel limits are real-valued/non-phase-sensitive and are often much more conservative with overestimation. Using these per-channel power limits, a second set of UPs (inversion and excitation) were designed for the self-built coil. Both SAR methods (per-channel power limits and EMF-based VOPs) were then used in a scan using the two sets of UPs and online FOCUS pulses for the self-built coil in the same volunteer. Conversely, a set of EMF-based VOPs could not be derived for the commercial coil because the coil model simulation was not available.

For all healthy volunteer scans, the predicted and real-time local SAR estimates for the pTx MPRAGE sequence were recorded in the scanner log system. Scanner measurements and SAR calculations performed offline were compared for both the EMF-based VOPs and fixed, per-channel power limits of SAR estimation methods.

2.3 | Parallel-transmit pulse design

Pulse design optimizations were performed with *MATLAB* R2020a (The MathWorks, Natick, MA, WA). The 5° excitation pulses (duration = 1 ms, 30-μs gradient ramp) were generated with the method described in Herrler et al.[9] The excitation pulses use an extended spiral nonselective (SPINS) gradient trajectory[20] and an energy regularization weight λ, as this strategy was previously proven stable.[9] Additionally, because the excitation pulse design falls within the STA approximation regime, complex RF pulse shapes could be calculated quickly and were sufficient to address the individual changes to B_1^+ and B_0 for the highly dynamic SPINS trajectory. The UP RF optimization was then calculated using the variable exchange algorithm[21] on eight training data sets altogether. Online customization of the RF shapes was performed with that same algorithm using the final UPs as starting points. All pTx excitation pulses were compared with a CP 5° excitation pulse of 100-μs duration, which was scaled accordingly using the mean reference voltage among all training data sets for comparability to UPs. For the additional 0.5-mm isotropic MPRAGE sequences performed in the self-built coil, FOCUS pulses were designed with stronger regularization of the specific energy dose (SED).

The pTx inversion pulses were based on a k_T-point trajectory[22] consisting of six k_T points. This trajectory was

15222594, 2023, 5, Downloaded from https://onlinelibrary.wiley.com/doi/10.1002/mrm.29569 by Universidad Rey Juan Carlos C/Tulipan S/N Edificio, Wiley Online Library on [24/01/2025]. See the Terms and Conditions (https://onlinelibrary.wiley.com/terms-and-conditions) on Wiley Online Library for rules of use; OA articles are governed by the applicable Creative Commons License

chosen to facilitate a large tip-angle (LTA) design. Despite the anticipated benefits of more complex trajectories,[23] a stable and fast online pulse design in the nonlinear LTA regime was only tractable when using the simpler k_T-point trajectory. The LTA optimization algorithm was an interior point–based algorithm proposed by Majewski[24] denoted as "IpOpt" below. The IpOpt optimizes RF magnitudes, phases, k_T-point locations, and subpulse durations under strict SED and gradient slew rate constraints. The first step of the optimization (k_T-point locations, subpulse durations, and RF magnitudes and phases) was calculated with the IpOpt using the eight training data sets combined. The initialization values were optimized without any SED constraints starting from six CP rectangular-shaped subpulses with channel magnitudes of 175 V and without any gradient blips.

In the next step, combined optimization variables (COVs) for the inversion pulse COV_{Inv} were defined. These included the transmit k-space locations of five of the six k_T-points (k_{Ti}, for $i \in \{1, 2, \dots, 5\}$ and $\dim \in \{x, y, z\}$), with the last k_T point always located in the center of transmit k-space. Additionally, a scaling factor c_{Tsub} for the subpulse durations was introduced (starting value = 1), and a limit for the local SED exposure in J/kg was imposed directly as SED_{lim}(starting value: SED estimate of an adiabatic HS4 pulse [duration = 12.8 ms, bandwidth = 1660 Hz] with nominal voltage of 350 V derived from the corresponding SAR supervision mode). In total, the inversion COVs contained the following parameters:

$$COV_{Inv} = \left[k_{T1,x}, k_{T1,y}, k_{T1,z}, \dots, k_{T5,z}, c_{Tsub}, SED_{lim}\right]. \quad (1)$$

To evaluate a single set of COVs, FOCUS pulses were designed with the IpOpt for each of the $N_p = 8$ training data sets. To assess the homogeneity of the FA distribution, a Bloch simulation was performed, and (FA-)NRMSE values for each individually optimized pulse p were calculated as

$$NRMSE_p = \frac{1}{N_v \alpha_t} \sum_{v=1}^{N_v} ||\alpha(v) - \alpha_t||_2^2. \quad (2)$$

Here, $\alpha(v)$ denotes the simulated FA in voxel v among N_v voxels in total, and α_t denotes the target FA of 180° for inversion. It has been shown that local FA dropouts may occur when using spokes or k_T points[25] and need to be considered by the optimization. Therefore, a basic brain extraction algorithm was performed after the optimization, and the minimum FA when neglecting the lowest second percentile within the brain, denoted as $\alpha_{\mathrm{min},p}$, was included in the universal offline optimization as a lower bound (see subsequently). To assess the pulse's contribution to the sequence's local SAR deposition, the corresponding maximum local SED value (SED_p) was calculated. To find the optimal COV_{Inv}, the following was minimized with the global search function from *MATLAB* (similar to equation 6 in Herrler et al[9]) with a time limit of 1 day:

$$\sum_{p=1}^{N_p} \exp\left(\frac{NRMSE_p\,(COV_{Inv}) - NRMSE_t}{NRMSE_t}\right) + \exp\left(\frac{\alpha_t - \alpha_{min,p}\,(COV_{Inv})}{\alpha_t}\right) + \exp\left(\frac{SED_p(COV) - SED_t}{SED_t}\right), \quad (3)$$

where target values $NRMSE_t = 0.05$, $\alpha_t = 180°$, and $SED_t = SED_{HS4,Unom=350V}$ in J/kg. This formula imposes exponentially weighted SED values, yet the COVs include a hard SED limit to find a more general tradeoff between local SED exposure and homogeneity. The initial UPs were then generated based on these optimized COV_{Inv} and using the IpOpt with all training data sets at once (same as the starting pulse for the optimization of COV_{Inv}). To calculate the UPs, 500 pseudo-randomly generated starting values were used to initialize the nonconvex IpOpt optimization. The starting values of the subpulses had both random RF magnitudes and phases (magnitudes are derived from the described initial Ups and multiplied by uniformly distributed numbers between 0.8 and 1.2; phases are uniformly distributed numbers between 0 and 2π). For each of the random initialization pulses, an IpOpt optimization was then performed with all training sets. The 500 resulting candidate solutions for the final UP were then associated with an NRMSE value using Equation (2), and the candidate corresponding to the lowest cost value was identified as the optimal solution.

For FOCUS pulses, B_1^+ and B_0 maps acquired at the beginning of the examination were exported to another computer and used for pulse design, as the IpOpt optimization was not fully integrated into the scanner software yet. The pulses were then reimported to the host computer to be played out by the sequences. It took approximately 13 s to customize an inversion pulse and about 9 s for an excitation pulse.

3 | RESULTS

3.1 | Simulation data

An evaluation of all pTx excitation pulses showed that the UPs performed worse regarding (FA-)NRMSE when used on the opposite coil for which it was generated. At the same time, all UP excitation pulses performed better than the CP excitation with a "universal" average scaling.

15222594, 2023, 5, Downloaded from https://onlinelibrary.wiley.com/doi/10.1002/mrm.29569 by Universidad Rey Juan Carlos C/Tulipan S/N Edificio, Wiley Online Library on [24/01/2025]. See the Terms and Conditions (https://onlinelibrary.wiley.com/terms-and-conditions) on Wiley Online Library for rules of use; OA articles are governed by the applicable Creative Commons License

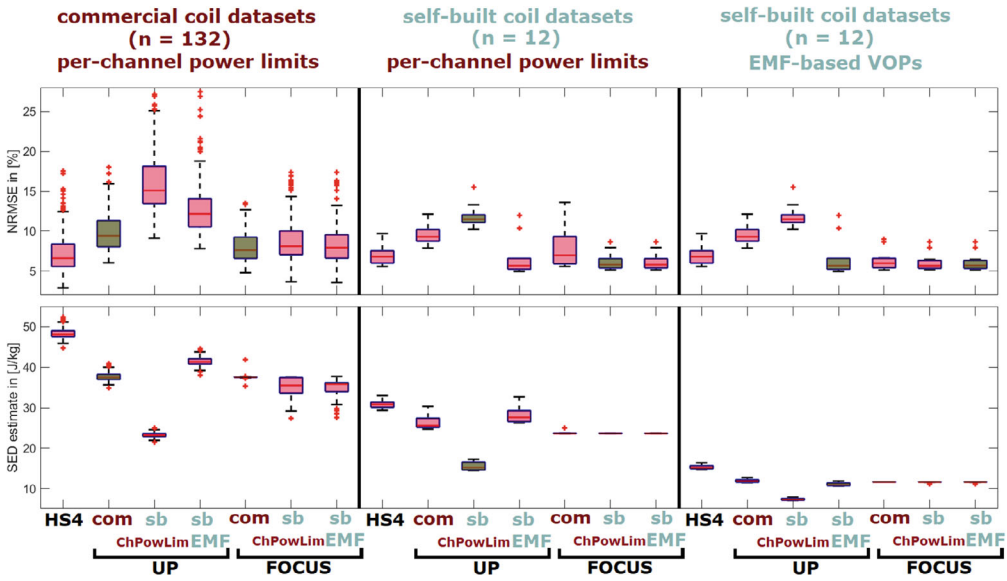

FIGURE 2 Flip-angle (FA) normalized RMS error (NRMSE) (top row) and SED estimates (bottom row) of adiabatic HS4 pulses (circularly polarized [CP]) with a nominal voltage of 400 V ($HS4_{400V}$), Ups, and FOCUS (parallel transmit [pTx]) inversion pulses. The UP and FOCUS pulses were derived from their own coil field map, and SAR data are colored green. The gain variation of the RF power amplifier was also taken into account, which led to a certain variation in SED among different subjects. (Left column) NRMSE and SED values using commercial coil data sets ($N = 132$) that use fixed channel power limits for SED estimation. (Center column) NRMSE and SED values using self-built coil data sets ($N = 12$) that use per-channel power limits for SED estimation. (Right column) NRMSE and SED values using self-built coil data sets ($N = 12$) that use VOPs for SED estimation. For data sets acquired with the commercial coil, $FOCUS_{com}$ achieves NRMSE values of < 12.45% in 95% of the volunteers, thereby showing the best robustness among all pulses. All FOCUS pulse performance increase when using electromagnetic field (EMF)–based VOPs. Generally, the VOP-based SED estimates of the self-built coil are lower than per-channel power limits of the same coil (52% lower) and the commercial coil (67% lower). When applied to the self-built coil and using EMF-based VOPs, all FOCUS pulses show very similar and good performance

When $FOCUS_{sb}$ pulses (subscript "sb" denotes optimization initialized with UPs of the self-built coil) are applied on the commercial coil, they show only slightly worse homogeneity but much higher SED than $FOCUS_{com}$ (subscript "com" denotes initialization with UPs of commercial coil). Importantly, the customization of all FOCUS pulses is always done for the subject and coil it is applied on.

The simulated NRMSE and SED values of all pTx inversion pulses and an HS4 adiabatic inversion CP pulse are shown in Figure 2 for data sets (B_1^+ maps, B_0 maps, VOPs) from both coils. To better distinguish the effects of using different coils versus different SAR supervision strategies, UP and FOCUS pulses were generated with self-built coil data sets but using per-channel power limits as well (subscripts "sb, ChPowLim" vs. EMF-based based "sb, EMF"). The nominal voltage for the adiabatic pulses was set to 400 V. This is lower than if set by the vendor-provided routine based on a transmitter voltage calibration, but is necessary to reduce SAR below the first level limit of 20 W/kg when using the per-channel power limits supervision. The proportion of commercial coil data sets in which $UP_{sb,EMF}$ shows lower NRMSE than UP_{com} was only 3.0%, but $FOCUS_{sb,EMF}$ outperformed $FOCUS_{com}$ in 28.8% of the commercial coil data sets. When using only brain voxels for customization, $FOCUS_{com}$/$FOCUS_{sb,EMF}$ reach NRMSE values of 3.2%/3.4% on average within the brain compared with 7.9%/8.5% in all valid voxels in commercial coil data sets. Notably, $UP_{sb,EMF}$ shows higher SED estimates than UP_{com} on commercial coil data sets but lower on self-built coil data sets. In general, the EMF-derived VOPs in the self-built coil provide approximately 52% lower SED estimations than the fixed per-channel power limits.

Figure 3 plots a pair of FOCUS excitation and inversion RF pulse and gradient waveforms designed for the self-built coil. For every time point of each of the pulses, the instantaneous pulse SED was calculated using the uncompressed electromagnetic-field simulation Q-matrices, the EMF-based VOPs (used in the self-built coil), and the "VOPs" enforcing fixed, per-channel power limits (used in commercial coil and also derived for the self-built coil). The SED for each respective calculation was then normalized to the maximum of the Q-matrices' value and plotted for comparison. As anticipated, EMF-based VOP estimates are greater than all Q-matrix SED values;

15222594, 2023, 5, Downloaded from https://onlinelibrary.wiley.com/doi/10.1002/mrm.29569 by Universidad Rey Juan Carlos C/Tulipan S/N Edificio, Wiley Online Library on [24/01/2025]. See the Terms and Conditions (https://onlinelibrary.wiley.com/terms-and-conditions) on Wiley Online Library for rules of use; OA articles are governed by the applicable Creative Commons License

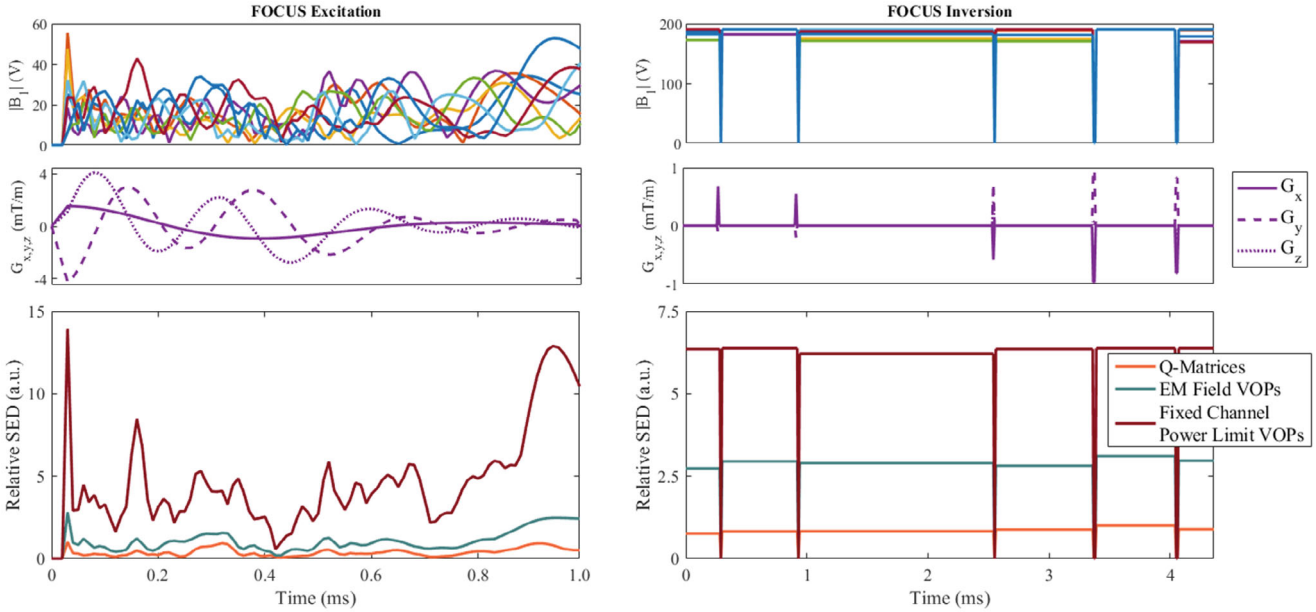

FIGURE 3 Comparison of RF waveforms, gradient waveforms, and relative instantaneous SED for FOCUS excitation (left) and inversion pulses (right) designed for the self-built coil. Magnitude pTx RF waveforms for eight transmit channels (top row). Excitation gradients for pTx waveforms (middle row). Time-resolved SED for both pulses calculated using the full EMF model Q-matrices before VOP compression (salmon orange), the compressed EMF VOPs used in the self-built coil (sea green), and the fixed per-channel power limit SAR monitoring method used in the commercial coil (crimson red) (bottom row). All relative SED is normalized to the maximum SED value of the Q-matrices' estimate

meanwhile, the per-channel power limit estimates are even greater still.

Figure 4 shows the simulated local SAR given a fixed 1-W input power for 10 000 uniformly distributed random shim 8-Tx configurations generated using *MATLAB*'s `rand/randi` functions. Each shim vector was normalized to unit norm length and used to estimate local SAR for the full EMF Q-matrices, the compressed EMF-based VOPs, and the fixed per-channel power limit VOP method—all based on the coil simulation of the self-built coil. The 1-W local SAR values for all configurations are displayed as histograms to show the distribution of local SAR values. Additionally, the local SAR for each configuration using uncompressed EMF Q-matrices and the compressed EMF-based VOPs were plotted against each other in a scatterplot to ensure the VOP overestimation condition held true for every simulated value. Finally, a one-to-one plot of the EMF-based and per-channel power limit local SAR is compared, showing that in nearly every case the per-channel power limits overestimate SAR compared with the EMF-based approach. One exception was found when the random vector had a Euclidean distance that was very close to the "worst case" configuration of the EMF-based VOPs, which is unique to the "worst case" derived from the uncompressed simulation to determine the per-channel power limits. In this case, the difference in SAR estimates was 0.01 W/kg.

3.2 | Experimental data

Figure 5 shows T_1-weighted MPRAGE images and corresponding simulated FA maps of 1 subject that were acquired with the commercial coil using various pulses for excitation and inversion.

Figure 6 displays a range of T_1-weighted MPRAGE images acquired for this study in multiple volunteers with the commercial and self-built pTx coil. For all volunteers, the same five scans are shown: HS4 adiabatic inversion with CP-mode excitation, UP_{com} pulses, $UP_{sb,\,EMF}$ pulses, $FOCUS_{com}$ pulses, and $FOCUS_{sb,\,EMF}$ pulses.

Local SAR measurements predicted by the 7T scanner are compared in Table 1 for both SAR management methods (EMF-based or fixed per-channel limits) in the self-built coil. In a single subject, MPRAGE scans with UPs and FOCUS pulses were repeated, applying both SAR supervision methods. In all cases, the local SAR reported using the EMF-based VOPs was lower than when using fixed, per-channel limits. In fact, the scanner operated within IEC local SAR normal mode (up to 10 W/kg in the head) for the EMF-based method, whereas it was within first level mode (10–20 W/kg) frequently for the per-channel limits approach.

Figure 7 compares the FOCUS pTx MPRAGE images in Subject 5 using the self-built coil at 1-mm^3 and 0.5-mm^3 isotropic resolution with EMF-based local SAR

15222594, 2023, 5, Downloaded from https://onlinelibrary.wiley.com/doi/10.1002/mrm.29569 by Universidad Rey Juan Carlos C/Tulipan S/N Edificio, Wiley Online Library on [24/01/2025]. See the Terms and Conditions (https://onlinelibrary.wiley.com/terms-and-conditions) on Wiley Online Library for rules of use; OA articles are governed by the applicable Creative Commons License

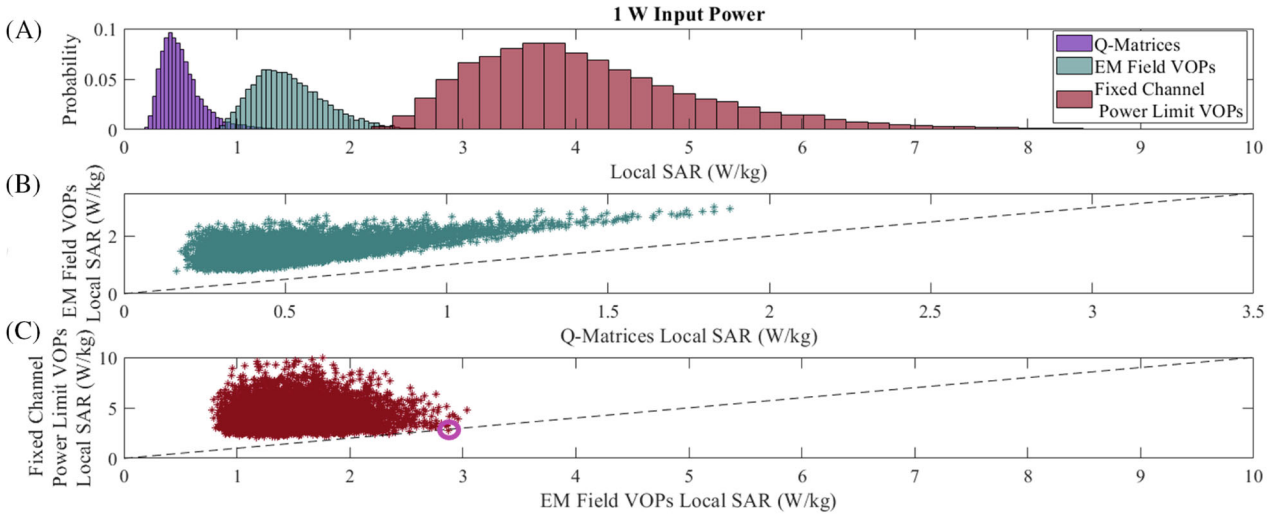

FIGURE 4 A, Histogram comparison of local SAR for full EMF simulation model Q-matrices (purple), VOPs compressed from electromagnetic (EM) simulation (sea green), and fixed per-channel power limit SAR monitoring derived for the same coil model (crimson red) across 10 000 random shim vectors applied with 1-W input power The x-axis shows the full distribution of local SAR across the three SAR estimate methods, which is dominated by the distribution from the fixed per-channel limit estimates. B, Local SAR estimates for the full Q-matrices (x-axis) against the EMF-based VOPs (y-axis) for the same shim configuration. As guaranteed by the VOP compression method, the EMF-based VOP estimates always overestimate SAR compared with the full uncompressed Q-matrices. C, Local SAR estimates for EMF-based VOPs (x-axis) compared with the per-channel power limits (y-axis). The only instance where the per-channel power limits are less conservative is a very specific vector that has the closest Euclidean distance to the EMF VOPs "worst case" vector compared with all other random vectors. This case is highlighted in the pink circle, and the local SAR value for the EMF-based VOP estimate is 2.78 W/kg, whereas the per-channel power limits is 2.77 W/kg

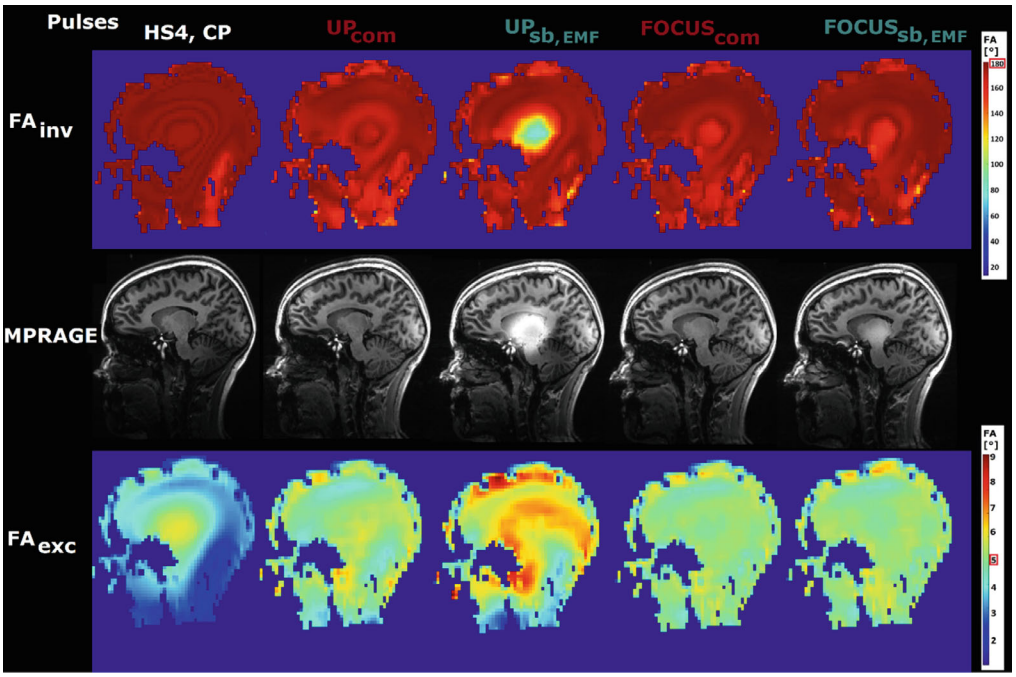

FIGURE 5 MPRAGE images acquired with the commercial coil and simulated corresponding FA maps of the used excitation and inversion pulses using either adiabatic HS4 + CP pulses as well as UPs or FOCUS pulses designed for the two different coils (subscript "com"/"sb" refer to commercial/self-built coil data sets used for the offline UP design). The adiabatic and UP_{com}/$FOCUS_{com}$ inversion pulses show no artifacts, whereas $UP_{sb,\ EMF}$/$FOCUS_{sb,\ EMF}$ show B_1^+-related artifacts in the center of the brain as well as B_0-related artifacts near the nasal cavity. All pTx excitation pulses show lower NRMSE values than the CP mode. In general, the agreement between the simulated inversion and excitation flip-angle maps and the experimental images is limited by the accuracy of the B_1^+ and B_0 maps. The accordance of the simulated maps and experimental images appears to be usable

15222594, 2023, 5, Downloaded from https://onlinelibrary.wiley.com/doi/10.1002/mrm.29569 by Universidad Rey Juan Carlos C/Tulipan S/N Edificio, Wiley Online Library on [24/01/2025]. See the Terms and Conditions (https://onlinelibrary.wiley.com/terms-and-conditions) on Wiley Online Library for rules of use; OA articles are governed by the applicable Creative Commons License

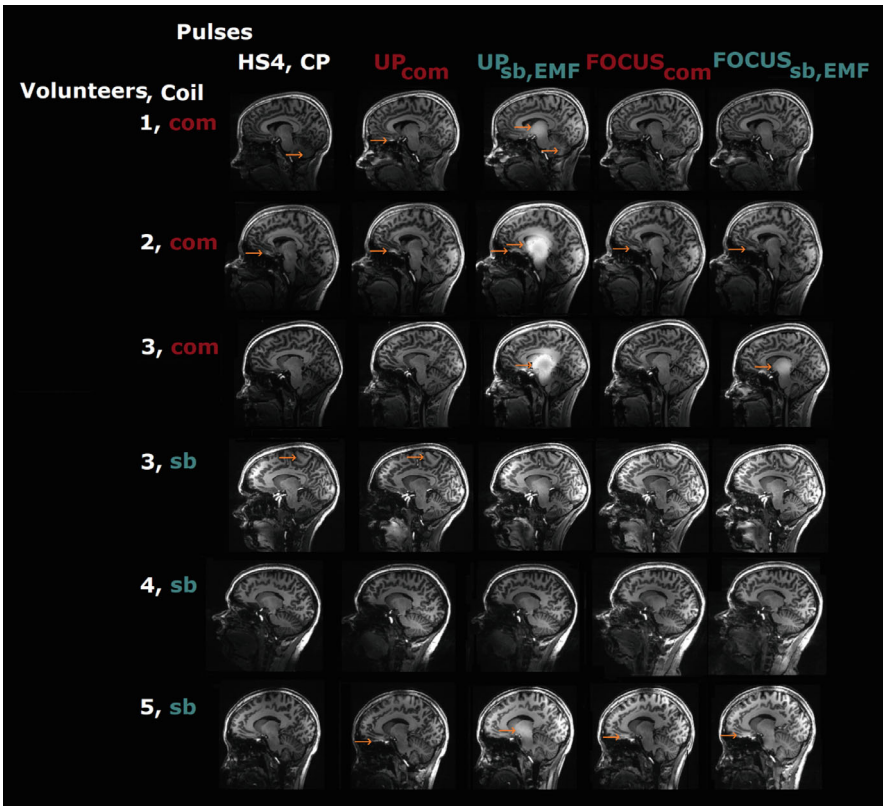

FIGURE 6 MPRAGE images of 3 subjects per coil using either adiabatic HS4 and CP pulses, UP, or FOCUS pulses optimized for both coils ("com" indicates the commercial coil, "sb" the self-built coil). Subject 3 was scanned with both coils. Image artifacts caused by imperfect pulse design are marked with orange arrows. As also indicated by Figure 2, adiabatic pulses and UPs for inversion show in the B_1^+ shading cerebellum of some subjects. UPs are generally prone to B_0-related artifacts near the paranasal sinus but also in the temporal lobe. When used by the commercial coil, UP_{sb} in particular shows poor inversion in the center of the brain, whereas UP_{com} still performs well when used by the self-built coil. FOCUS pulses show more comparable and robust performance across different subjects, as well as less-severe B_0-related artifacts

TABLE 1 Comparison of experimental local SAR predictions measured by the scanner in the pTx MPRAGE sequence for both SAR management methods (EMF-based VOPs and per-channel power limits)

pTx MPRAGE pulses	EMF-based VOPs % max local SAR	ChPowLim limits % Max local SAR	Ratio ChPowLim limits/ EMF-based VOPs
UPs EMF	27.3	52.3	1.92
UPs ChPowLim	21.6	42.9	1.99
FOCUS EMF	35.5	76.4	2.15
FOCUS ChPowLim	32.2	63.3	1.97

Note: All local SAR values are listed as a percentage of the maximum permitted (20 W/kg for first-level mode). All pulses were designed for and used in the self-built pTx coil and the same subject. The following four MPRAGE scans were performed twice: UP inversion and excitation designed with EMF-based VOPs, UP inversion and excitation designed with fixed per-channel power limits, FOCUS inversion and excitation initialized with the EMF-based UPs, and FOCUS inversion and excitation initialized with the fixed per-channel power limits UPs. In the first series of scans, the local SAR was supervised with the EMF-based VOPs (values in second column), and in the second series of same scans, the fixed per-channel power limit supervision was used (values in third column). The ratio of these two scanner local SAR estimates are reported in the last column.

supervision only. The yellow box windows show a zoomed region that highlights the increase in resolution for each plane of view. With the higher resolution, the length of the readout train increases with the 0.5-mm^3 acquisition, which changes the T_1-weighted contrast in the image.

4 | DISCUSSION

In this work we extended the concept of universal optimization and online customization to the LTA domain and developed clinically applicable pTx inversion pulses based on 6 k_T points that use individually optimized gradient and RF pulse shapes. Their robust performance was shown for $N = 132$ commercial coil and $N = 12$ self-built coil data sets and may allow them to serve as a low-SAR alternative to adiabatic inversion pulses. PTx UPs and FOCUS pulses designed for excitation consisted of a SPINS gradient trajectory and online-customized RF shapes. The comparison of UP and FOCUS pTx excitation and inversion pulses was evaluated in two separate 8-Tx RF head coils of similar design: one self-built and one provided commercially. Along with pulse performance, the use of two different SAR supervision strategies of the coils was compared.

When applied on a distinct coil to the one used for pulse optimization, we found strong artifacts with UPs for particular subjects. For example, in Figure 5 the UP inversion pulse designed for the self-built coil produced an

15222594, 2023, 5, Downloaded from https://onlinelibrary.wiley.com/doi/10.1002/mrm.29569 by Universidad Rey Juan Carlos C/Tulipan S/N Edificio, Wiley Online Library on [24/01/2025]. See the Terms and Conditions (https://onlinelibrary.wiley.com/terms-and-conditions) on Wiley Online Library for rules of use; OA articles are governed by the applicable Creative Commons License

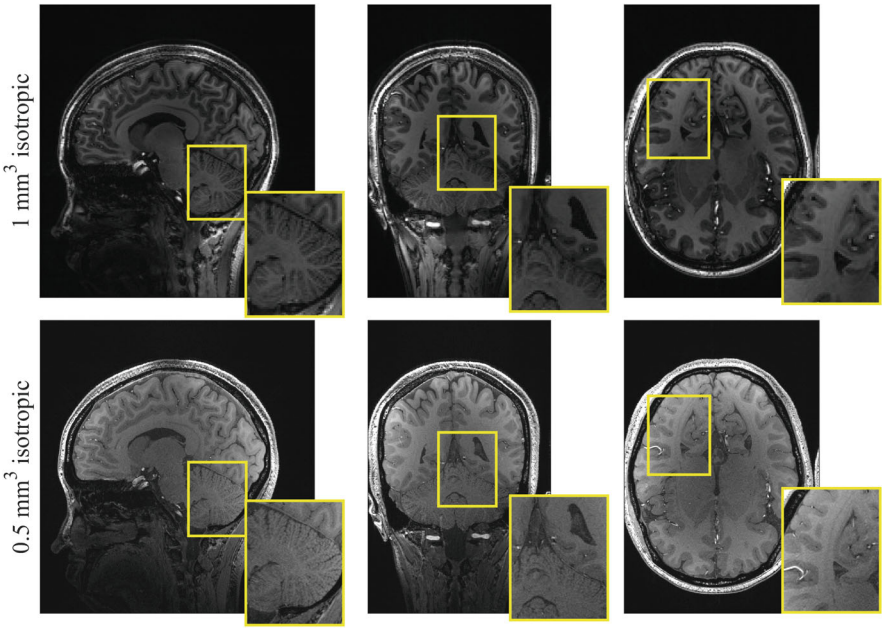

FIGURE 7 Comparison of MPRAGE images using the self-built pTx coil in the same volunteer acquired with FOCUS pulses and SAR supervision EMF-based VOPs. Images with 1-mm^3 isotropic (acquisition time [TA] = 4 min 56 s) (top row) and with 0.5-mm^3 isotropic resolution (TA = 9 min 15 s) (bottom row). Yellow boxes capture a zoomed region to appreciate the resolution differences. The difference in T_1 contrast between the two resolutions is attributed to the longer readout time for the 0.5-mm^3 acquisition. The same higher-resolution 0.5-mm^3 scan was not possible in the commercial coil due to more restrictive SAR management with fixed per-channel power limits

artifact in the center of the brain when used on the commercial coil. In a previous study, both coils had very similar B_1^+ fields when compared with the same imaging phantom, yet the self-built coil had an approximate 10% reduction in peak B_1^+ attributed to the RF shield eye cutouts.[17] Meanwhile, FOCUS pulses show more stable performance when designed from the opposite coil UP, yet still perform worse than when designed from the native coil UP.

The performance of pTx pulses not only varied with the coil used in its design, but also with the subject's geometry and anatomy. Just like in the original description of UPs,[4] the largest variation was observed with improper patient positioning, in which all pTx pulses were unable to effectively homogenize the entire brain (Figure S1). This variation in performance was also seen in CP adiabatic pulses, which is likely due to an unmet adiabatic condition due to SAR restrictions, as shown in some subjects in Figure 6. Therefore, we suspect that, if possible, it is more desirable to use a FOCUS approach with pulse optimization tailored to the individual. An interesting future comparison would be to compare the FOCUS method with another recent subject-specific technique, SUPs.[8]

The SAR supervision comparison studied the VOP approach derived from EMF simulations and fixed transmit channel power limits as a proxy for VOPs. The EMF-based VOPs are only used in the self-built 8-Tx coil in this study and are derived from simulations from 3 subjects at three different positions each with a VOP worst-case overestimation factor of 25% and additional safety factors. The per-channel power limit approach was used in the commercial 8-Tx coil and derived for the self-built coil as well. For the EMF-based case, there were 15 local SAR VOPs, and in the per-channel limit case, 8 local "VOP" checkpoints, resulting in the same order of magnitude complexity for SAR calculations online and SAR constraints or regularization in offline pulse design. The EMF-based VOP management led to consistently lower SAR values than the fixed transmit channel power limits method in both coils, while still maintaining reliable overestimation and computational feasibility. Although the coil model is not available for the commercial coil, the intermediate comparison of both SAR management methods in the self-built coil allowed for some separation of coil design/performance characteristics and SAR estimation differences.

Furthermore, using the EMF-based SAR supervision and pTx inversion pulses, a set of 1-mm^3 isotropic MPRAGE sequences and 0.5-mm^3 isotropic resolution sequences could be acquired within local SAR estimations below the IEC limits for head imaging in normal mode operation (10 W/kg). These sequences could only be acquired in first-level mode (up to 20 W/kg) when using the commercial coil's local SAR management. While the self-built coil only required scans to operate within normal mode for the pTx pulses designed, it is also possible that pulses with higher respective SED values could be calculated for better pulse performance in terms of NRMSE due to the inherent trade-off between pulse design accuracy and SED penalization during optimization. A comparison of the two SAR management methods both operating within first-level mode could further support the benefits of using EMF-based VOPs. Additionally, $UP_{sb,\,EMF}$ generated higher SED estimates than UP_{com} and $UP_{sb,\,ChPowLim}$ when evaluated using per-channel power limits for estimation, but lower when using EMF-based VOPs. This indicates that using EMF-based VOPs in pTx pulse design

15222594, 2023, 5, Downloaded from https://onlinelibrary.wiley.com/doi/10.1002/mrm.29569 by Universidad Rey Juan Carlos C/Tulipan S/N Edificio, Wiley Online Library on [24/01/2025]. See the Terms and Conditions (https://onlinelibrary.wiley.com/terms-and-conditions) on Wiley Online Library for rules of use; OA articles are governed by the applicable Creative Commons License

may lead to a better distribution of local SAR exposure across the head.

Despite the SAR and performance advantages they offer, pTx inversion pulses in some cases show small B_0-related artifacts at air–tissue interfaces near the nasal cavity or the inner ear. Furthermore, poor inversion was achieved in the center of the brain for some cases as well. These two types of artifacts did not match very well with the corresponding FA simulations and may be related to the limited accuracy of the B_1^+ and B_0 maps or patient movement. In fact, a major limitation of the FOCUS approach in general is the requirement of fast but accurate B_1^+ and B_0 mapping sequences, which is not the case for UPs.

To overcome these artifacts, several future adaptations could be implemented. First, B_1^+ and B_0 map accuracy could be enhanced by correction methods and more advanced sequences.[26–30] Second, B_1^+ maps could additionally be corrected with an estimation of motion-induced changes in the B_1^+ field[31] during the measurement. Furthermore, pTx inversion pulses could be designed to be more robust to B_0 offsets, such as by introducing weighted B_0 uncertainties or offsets into the pulse calculation.[23] Finally, a brain extraction algorithm (to remove scalp and other non-brain tissue) may be used for all field maps before performing any pulse design. This could potentially lead to lower SED values for the pulses because B_1^+ intensity in non-brain tissues is likely to be lower on average, meaning it contributes to larger power deposition when included in a design. Another favorable result of such a brain extraction might be better homogeneity inside the brain tissue, yet the FA may consequently drop severely in non-brain tissues, rendering them invisible. Conversely, this could be problematic if these tissues were deemed clinically relevant for certain diagnoses.

Because FOCUS pulses are designed online, they impose certain SED limits to ensure predictable SAR values for any sequence that uses these pulses. These limits could therefore be set to the SED of a corresponding CP pulse, thereby guaranteeing that every sequence protocol that runs in CP mode will also run in pTx mode. To maintain short online calculation times, the use of machine learning in combination with more complex RF pulse and gradient shapes may become necessary.[32–34] On the other hand, using a fixed SPINS trajectory or k_T-point trajectory with rectangular RF subpulse shapes have shown to serve as a rather simple solution, permitting individual optimization in real time. With additional degrees of freedom, more complex gradient and RF pulse shapes may introduce more local minima in the nonconvex joint optimization problem, placing heavier reliance on well-chosen starting values for an individual optimization.

Short calculation times become harder to maintain when sequences use several different pulses. For example, 2D sequences must mitigate different field distributions for slice-selective pulses. The application of 2D UPs has only yet been achieved for STA pulses with fixed slice configurations.[10] "MetaPulse2D" is a recent customized approach that adapts slice-selective UPs created for rigid slice positions to arbitrary slice orientations and positions.[35] Another recent approach replaces the UP with several cluster-specific pulses that are used as a warm start.[36] From there, neural networks quickly choose the best fitting cluster for every slice online by predicting every pulse's potential FA distribution with FOCUS optimization. In combination with two-spoke excitation pulses designed with strict SAR constraints, short online calculation times were achieved on an external computer. Another example of sequences with many pulses are turbo spin echo (RARE/TSE/FSE) sequences.[37] These sequences may benefit from a combination of FOCUS excitation pulses and a universal train of refocusing pulses optimized with the direct signal control with variable excitation and refocusing pulses (DiSCoVER) method,[38,39] where online customization to addresses protocol changes during the examination.[40] While universal solutions have already been shown for 2D sequences with multiple RF pulses, these recent individual approaches still need evaluation in clinical populations.

The dependency on initialization values for FOCUS pulses was originally shown in Herrler et al.[9] but also in this paper when comparing FOCUS pulses across two RF coils. For excitation, the pTx pulse (UP or FOCUS pulse) designed for the RF coil was the better choice in almost every case, yet this was not always true for inversion pulses. In fact, the pTx inversion UP designed for the other coil would have been the better choice for a non-negligible number of subjects (~28%), which highlights the challenges of the LTA joint optimization and limitations of using a single UP as warm start for individual optimization. One potential solution might be to develop a clustering algorithm that selects the best choice for each subject among several previously generated pulses based on the previously acquired B_1^+ and B_0 maps akin to what was presented in Herrler et al.[36] and Tomi-Tricot et al.[41]

5 | CONCLUSIONS

We have presented universal and online-customized excitation and inversion pTx pulses for two 8-Tx head coils with distinct SAR management VOPs at 7 T. Using the MPRAGE sequence, we evaluated their benefit in terms of RF homogeneity and estimations of local SAR exposure using the two pTx coils. In addition to Ups, FOCUS

15222594, 2023, 5, Downloaded from https://onlinelibrary.wiley.com/doi/10.1002/mrm.29569 by Universidad Rey Juan Carlos C/Tulipan S/N Edificio, Wiley Online Library on [24/01/2025]. See the Terms and Conditions (https://onlinelibrary.wiley.com/terms-and-conditions) on Wiley Online Library for rules of use; OA articles are governed by the applicable Creative Commons License

inversion pulses consist of relatively simple gradient and RF pulse shapes and may serve as a low-SAR alternative to the commonly used adiabatic pulses. When trained on a distinct coil from the coil that is used, FOCUS pulses achieve slightly better performance to Ups. FOCUS pulses for inversion generalize a bit better across different 8-Tx head coils than UPs. Furthermore, using EMF simulations to manage local SAR with VOPs can provide significant advantages in terms of local SAR estimation, while always providing an overestimation of the ground-truth local SAR for safety considerations. In the case of MPRAGE with pTx excitation and inversion used in this study, EMF-based local SAR management enables high-resolution sequences that still meet the IEC limits for head imaging in normal mode operation.

ACKNOWLEDGMENT

The authors thank John E. Foster, Tracey Hopkins, and Rosemary Woodward (NHS Greater Glasgow & Clyde, Glasgow, UK) for their support with the safety validation of the self-built coil and the volunteer scanning in this study. David A. Porter and Armin M. Nagel contributed equally to this work. Open Access funding enabled and organized by Projekt DEAL.

CONFLICT OF INTEREST

Jürgen Herrler, Patrick Liebig, Christian Meixner, and Rene Gumbrecht are employees of Siemens Healthcare (Germany); Belinda Ding is an employee of Siemens Healthcare (UK); and Shajan Gunamony is the founder and director of MR CoilTech.

DATA AVAILABILITY STATEMENT

The Universal Pulses used in this study (excitation and inversion for both self-built and commercial coils) are available for download at https://github.com/JuiHerrler/PTx-pulse-data.

ORCID

Jürgen Herrler https://orcid.org/0000-0002-4620-8216
Sydney N. Williams https://orcid.org/0000-0001-9979-6245
Patrick Liebig https://orcid.org/0000-0001-7342-3715
Christian R. Meixner https://orcid.org/0000-0003-2799-6277
Shajan Gunamony https://orcid.org/0000-0002-3146-6079
David A. Porter https://orcid.org/0000-0001-8436-6904
Armin M. Nagel https://orcid.org/0000-0003-0948-1421

REFERENCES

1. Ladd ME, Bachert P, Meyerspeer M, et al. Pros and cons of ultra-high-field MRI/MRS for human application. *Prog NMR Spectro.* 2018;109:1-50.
2. Pauly JM, Nishimura DG, Macovski A. A k-space analysis of small-tip angle excitation. *J Magn Reson.* 1989;81:43-56.
3. Katscher U, Börnert P, Leussler C, van den Brink JS. Transmit SENSE. *Magn Reson Med.* 2003;49:144-150.
4. Gras V, Vignaud A, Amadon A, Le Bihan D, Boulant N. Universal pulses: a new concept for calibration-free parallel transmission. *Magn Reson Med.* 2017;77:635-643.
5. Gras V, Mauconduit F, Vignaud A, et al. Design of universal parallel-transmit refocusing kT-point pulses and application to 3D T_2-weighted imaging at 7T. *Magn Reson Med.* 2018;80:53-65.
6. Gras V, Pracht ED, Mauconduit F, Le Bihan D, Stöcker T, Boulant N. Robust nonadiabatic T_2 preparation using universal parallel-transmit k_T-point pulses for 3D FLAIR imaging at 7T. *Magn Reson Med.* 2019;81:3202-3208.
7. Aigner CS, Dietrich S, Schmitter S. Three-dimensional static and dynamic parallel transmission of the human heart at 7T. *NMR Biomed.* 2021;34:e4450.
8. Le Ster C, Mauconduit F, Massire A, Boulant N, Gras V. Standardized universal pulse: a fast RF calibration approach to improve flip angle accuracy in parallel transmission. *Magn Reson Med.* 2022;87:2839-2850.
9. Herrler J, Liebig P, Gumbrecht R, et al. Fast online-customized (FOCUS) parallel transmission pulses: a combination of universal pulses and individual optimization. *Magn Reson Med.* 2021;85:3140-3153.
10. Gras V, Boland M, Vignaud A, et al. Homogeneous non-selective and slice-selective parallel-transmit excitations at 7 tesla with universal pulses: a validation study on two commercial RF coils. *PLoS One.* 2017;12:e0183562.
11. Vaughan JT, Garwood M, Collins CM, et al. 7T vs. 4T: RF power, homogeneity, and signal-to-noise comparison in head images. *Magn Reson Med.* 2001;46:24-30.
12. Lee J, Gebhardt M, Wald LL, Adalsteinsson E. Local SAR in parallel transmission pulse design. *Magn Reson Med.* 2012;67:1566-1578.
13. *Medical Electrical Equipment—Particular Requirements for the Safety of Magnetic Resonance Equipment for Medical Diagnosis*. International Electrotechnical Commission; 2010.
14. Graesslin I, Homann H, Biederer S, et al. A specific absorption rate prediction concept for parallel transmission MR. *Magn Reson Med.* 2012;68:1664-1674.
15. Eichfelder G, Gebhardt M. Local specific absorption rate control for parallel transmission by virtual observation points. *Magn Reson Med.* 2011;66:1468-1476.
16. Mugler JP, Brookeman JR. Three dimensional magnetization-prepared rapid gradient-echo imaging (3D MP-RAGE). *Magn Reson Med.* 1990;15:152-157.
17. Williams SN, Allwood-Spiers S, McElhinney P, et al. A nested eight-channel transmit array with open-face concept for human brain imaging at 7 tesla. *Frontier Phys.* 2021;9:701330.
18. Fautz H-P, Vogel M, Gross P, Kerr AB, Zhu Y. B1 mapping of coil arrays for parallel transmission. *Proceedings of the 16th Annual Meeting of ISMRM*, ISMRM, Toronto, 2008:1247.
19. Boulant N, Gras V, Amadon A, Luong M, Ferrand G, Vignaud A. Workflow proposal for defining SAR safety margins in parallel transmission. *Proceedings of the 26th Annual Meeting of ISMRM*, ISMRM, Paris, 2018:295.
20. Malik SJ, Keihaninejad S, Hammers A, Hajnal JV. Tailored excitation in 3D with spiral nonselective (SPINS) RF pulses. *Magn Reson Med.* 2012;67:1303-1315.

15222594, 2023, 5, Downloaded from https://onlinelibrary.wiley.com/doi/10.1002/mrm.29569 by Universidad Rey Juan Carlos C/Tulipan S/N Edificio, Wiley Online Library on [24/01/2025]. See the Terms and Conditions (https://onlinelibrary.wiley.com/terms-and-conditions) on Wiley Online Library for rules of use; OA articles are governed by the applicable Creative Commons License

21. Setsompop K, Wald LL, Alagappan V, Gagoski BA, Adalsteinsson E. Magnitude least squares optimization for parallel radio frequency excitation design demonstrated at 7 tesla with eight channels. *Magn Reson Med.* 2008;59:908-915.
22. Cloos MA, Boulant N, Luong M, et al. kT-points: short three-dimensional tailored RF pulses for flip-angle homogenization over an extended volume. *Magn Reson Med.* 2012;67:72-80.
23. Van Damme L, Mauconduit F, Chambrion T, Boulant N, Gras V. Universal nonselective excitation and refocusing pulses with improved robustness to off-resonance for magnetic resonance imaging at 7 tesla with parallel transmission. *Magn Reson Med.* 2021;85:678-693.
24. Majewski K. Simultaneous optimization of radio frequency and gradient waveforms with exact hessians and slew rate constraints applied to kT-points excitation. *J Magn Reson.* 2021;326:106941.
25. Paez A, Gu C, Cao Z. Robust RF shimming and small-tip-angle multispoke pulse design with finite-difference regularization. *Magn Reson Med.* 2021;86:1472-1481.
26. Yarnykh VL. Actual flip-angle imaging in the pulsed steady state: a method for rapid three-dimensional mapping of the transmitted radiofrequency field. *Magn Reson Med.* 2007;57:192-200.
27. Eggenschwiler F, Kober T, Magill AW, Gruetter R, Marques JP. SA2RAGE: a new sequence for fast B1+-mapping. *Magn Reson Med.* 2012;67:1609-1619.
28. Nehrke K, Börnert P. DREAM-a novel approach for robust, ultrafast, multislice B_1^+ mapping. *Magn Reson Med.* 2012;68:1517-1526.
29. Padormo F, Hess AT, Aljabar P, et al. Large dynamic range relative B_1^+ mapping. *Magn Reson Med.* 2016;76:490-499.
30. Hess AT, Dragonu I, Chiew M. Accelerated calibrationless parallel transmit mapping using joint transmit and receive low-rank tensor completion. *Magn Reson Med.* 2021;86:2454-2467.
31. Plumley A, Watkins L, Treder M, Liebig P, Murphy K, Kopanoglu E. Rigid motion-resolved prediction using deep learning for real-time parallel-transmission pulse design. *Magn Reson Med.* 2022;87:2254-2270.
32. Ianni JD, Cao Z, Grissom WA. Machine learning RF shimming: prediction by iteratively projected ridge regression. *Magn Reson Med.* 2018;80:1871-1881.
33. Shin D, Kim Y, Oh C, et al. Deep reinforcement learning-designed radiofrequency waveform in MRI. *Nat Mach Intel.* 2021;3:985-994.
34. Vinding MS, Aigner CS, Schmitter S, Lund TE. DeepControl: 2DRF pulses facilitating inhomogeneity and B_0 off-resonance compensation in vivo at 7 T. *Magn Reson Med.* 2021;85:3308-3317.
35. Macounduit F, Gras V, Vignaud A, Boulant N. MetaPulse2D: methodology to enable universal slice specific spokes pulses in parallel transmission. *Proceedings of the 30th Annual Meeting of ISMRM*, ISMRM, London, 2022:454.
36. Herrler J, Liebig P, Majewski K, et al. Neural network-supported fast online-customized (FOCUS) parallel transmit (pTx) pulses for slice-selective, large tip angle excitation. *Proceedings of the 30th Annual Meeting of ISMRM*, ISMRM, London, 2022:3312.
37. Hennig J, Nauerth A, Friedburg H. RARE imaging: a fast imaging method for clinical MR. *Magn Reson Med.* 1986;3:822-833.
38. Malik SJ, Beqiri A, Padormo F, Hajnal JV. Direct signal control of the steady-state response of 3D-FSE sequences. *Magn Reson Med.* 2015;73:951-963.
39. Beqiri A, Hoogduin H, Sbrizzi A, Hajnal JV, Malik SJ. Whole-brain 3D FLAIR at 7T using direct signal control. *Magn Reson Med.* 2018;80:1533-1545.
40. Herrler J, Endres J, Tomi-Tricot R, et al. Direct signal control combined with dymanic, fast online customized (FOCUS), parallel transmit excitation pulses for TSE at 7 Tesla. *Proceedings of the 30th Annual Meeting of ISMRM*, ISMRM, London, 2022:3313.
41. Tomi-Tricot R, Gras V, Thirion B, et al. SmartPulse, a machine learning approach for calibration-free dynamic RF shimming: preliminary study in a clinical environment. *Magn Reson Med.* 2019;82:2016-2031.

SUPPORTING INFORMATION

Additional supporting information may be found in the online version of the article at the publisher's website.

Figure S1. Example of a volunteer MPRAGE scan where the subject was not fully positioned in the self-built coil. The left column shows circularly polarized (CP) excitation and adiabatic inversion with a reference voltage of 400 V. The center column used parallel-transmit (pTx) excitation and inversion universal pulses (Ups) derived for the self-built coil. The right column used pTx excitation and inversion fast online-customized (FOCUS) pulses derived from the self-built coil UPs. A, On the left-hand side of the brain, the cerebellum has lost anatomical detail with CP pulses (red arrow), shows some improvement with UPs (orange arrow), but has recovered homogeneity with FOCUS pulses (green arrow). B, On the right-hand side of the brain, the poor signal and artifacts in the cerebellum appear again in the CP pulses (red arrow). These artifacts cannot be corrected with UPs nor even FOCUS (orange arrows)

How to cite this article: Herrler J, Williams SN, Liebig P, et al. The effects of RF coils and SAR supervision strategies for clinically applicable nonselective parallel-transmit pulses at 7 T. *Magn Reson Med*. 2023;89:1888-1900. doi: 10.1002/mrm.29569

15222594, 2023, 5, Downloaded from https://onlinelibrary.wiley.com/doi/10.1002/mrm.29569 by Universidad Rey Juan Carlos C/Tulipan S/N Edificio, Wiley Online Library on [24/01/2025]. See the Terms and Conditions (https://onlinelibrary.wiley.com/terms-and-conditions) on Wiley Online Library for rules of use; OA articles are governed by the applicable Creative Commons License